Efficient Simulation of large polaritonic systems

M. Elious Mondal[1, a)] and Pengfei Huo[1, 2, b)]
[1)] *Department of Chemistry, University of Rochester, Rochester, New York, 14627, USA*
[2)] *The Institute of Optics, Hajim School of Engineering, University of Rochester, Rochester, NY 14627, USA*

We demonstrate an efficient way(s) to simulate the 2DES of polaritonic systems for the HTC Hamiltonian. This when combined with the forward-backward nature of PLDM, helps to simplify and make 2DES calculations of large polaritonic systems (large number of molecules) feasible, which is needed to study the collective coupling in polaritons. A lot of these tricks can be used for increasing the efficiency of general semicalssical trajectory based methods for density matrix dynamics and sprectroscopic calculations.

I. INTRODUCTION

II. THEORY

We demonstrate the strategies to efficiently manipulate matrix-vector multiplications to reduce the computation cost of semiclassical simulations. We consider the Hilbert space upto the second excitation subspace with $\mathcal{O}(N^2)$ states for N-molecule polaritonic system. We first demonstrate how the action of hamiltonian on a wavefunction can be written as the sum of simple hadamard product of vectors which reduces the matrix-vector multiplication from $\mathcal{O}(N^4)$ to $\mathcal{O}(N^2)$. We use a similar modification for the action of dipole operator on the wavefunction. This simplified action allows us to develop a simple procedure for focusing step in the PLDM-spectra calculation which helps us to avoid the generation of any density matrix and also simplifies response function calculations. Finally we demonstrate how the above tools can be efficiently used to vectorize over trajectories(or pulses) to further reduce the total computational cost of high-dimensional spectroscopy calculations.

A. HΨ

We use the HTC hamiltonian to describe a system of N-molecules (emitters) coupled to single cavity mode.

$$\begin{aligned}\hat{H}_{\mathrm{HTC}} =& \sum_i (\hbar\omega_i + \lambda)\hat{\sigma}_i^\dagger\hat{\sigma}_i + \hbar\omega_{\mathrm{c}}\hat{a}^\dagger\hat{a} + \hbar g_{\mathrm{c}}\sum_i(\hat{\sigma}_i^\dagger\hat{a} + \hat{\sigma}_i\hat{a}^\dagger) \\ &+ \sum_{i,\nu}\hbar\omega_\nu\left(\hat{b}_{i,\nu}^\dagger\hat{b}_{n,\nu} + \frac{1}{2}\right) + \sum_{i,\nu}c_{i,\nu}\hat{\sigma}_i^\dagger\hat{\sigma}_i\left(\hat{b}_{i,\nu}^\dagger + \hat{b}_{i,\nu}\right)\end{aligned} \tag{1}$$

Here, $\hat{\sigma}_i^\dagger(\hat{\sigma}_i)$ creates(destroys) an excitation on the i^{th} molecule and $\hat{a}_i^\dagger(\hat{a}_i)$ creates(destroys) an excitation on the photon mode. We also consider diagonal fluctuations in the molecules due to bilinear exciton-phonon coupling of molecules with their individual phonon bath. For the semiclassical dynamics, we treat the phonons semiclassically within the PLDM framework and sample the phonon modes from a spectral density. In the double excitation subspace, we define the diabatic exciton-photon basis,

$$\left|\mathrm{E}_i^0\right\rangle = \left(\bigotimes_{j\neq i}\left|\mathrm{g}_j\right\rangle\right)\otimes\left|\mathrm{e}_i\right\rangle\otimes\left|0\right\rangle \tag{2}$$

$$\left|\mathrm{G}^1\right\rangle = \left(\bigotimes_{i}\left|\mathrm{g}_i\right\rangle\right)\otimes\left|1\right\rangle \tag{3}$$

$$\left|\mathrm{E}_{ij}^0\right\rangle = \left(\bigotimes_{k\neq i,j}\left|\mathrm{g}_j\right\rangle\right)\otimes\left|\mathrm{e}_i\right\rangle\otimes\left|\mathrm{e}_j\right\rangle\otimes\left|0\right\rangle \tag{4}$$

$$\left|\mathrm{E}_i^1\right\rangle = \left(\bigotimes_{j\neq i}\left|\mathrm{g}_j\right\rangle\right)\otimes\left|\mathrm{e}_i\right\rangle\otimes\left|1\right\rangle \tag{5}$$

$$\left|\mathrm{G}^2\right\rangle = \left(\bigotimes_{i}\left|\mathrm{g}_i\right\rangle\right)\otimes\left|2\right\rangle \tag{6}$$

With the above basis, the HTC hamiltonian (62) can be written as

$$\begin{aligned}\hat{H}_{\mathrm{HTC}} =& \sum_i \epsilon_{\mathrm{E}_i^0}\left|\mathrm{E}_i^0\right\rangle\!\left\langle\mathrm{E}_i^0\right| + \omega_{\mathrm{c}}\left|\mathrm{G}^1\right\rangle\!\left\langle\mathrm{G}^1\right| + 2\omega_{\mathrm{c}}\left|\mathrm{G}^2\right\rangle\!\left\langle\mathrm{G}^2\right| + \\ &\sum_{i,j>i}\epsilon_{\mathrm{E}_{ij}^0}\left|\mathrm{E}_{ij}^0\right\rangle\!\left\langle\mathrm{E}_{ij}^0\right| + \sum_i\epsilon_{\mathrm{E}_i^1}\left|\mathrm{E}_i^1\right\rangle\!\left\langle\mathrm{E}_i^1\right| + \\ & g_{\mathrm{c}}\sum_i\left(\left|\mathrm{E}_i^0\right\rangle\!\left\langle\mathrm{G}^1\right| + \sqrt{2}\left|\mathrm{E}_i^1\right\rangle\!\left\langle\mathrm{G}^2\right| + \sum_{j>i}\left|\mathrm{E}_{ij}^0\right\rangle\!\left\langle\mathrm{E}_i^1\right| + h.c.\right)\end{aligned} \tag{7}$$

A general wavefunction can be expanded in this double-excitation subspace as

$$\begin{aligned}\left|\Psi\right\rangle =& c_{\mathrm{G}^0}\left|\mathrm{G}^0\right\rangle + \sum_i c_{\mathrm{E}_i^0}\left|\mathrm{E}_i^0\right\rangle + c_{\mathrm{G}^1}\left|\mathrm{G}^1\right\rangle + \\ &\sum_{i,j>i}c_{\mathrm{E}_{ij}^0}\left|\mathrm{E}_{ij}^0\right\rangle + \sum_i c_{\mathrm{E}_i^1}\left|\mathrm{E}_i^1\right\rangle + c_{\mathrm{G}^2}\left|\mathrm{G}^2\right\rangle\end{aligned} \tag{8}$$

where $c_{\mathrm{m}} = \langle\mathrm{m}|\Psi\rangle$. From now onwards, we follow the basis ordering,

$$\Psi \rightarrow \left[c_{\mathrm{G}^0}, c_{\mathrm{E}_i^0}, c_{\mathrm{G}^1}, c_{\mathrm{E}_{ij}^0}, c_{\mathrm{E}_i^1}, c_{\mathrm{G}^2}\right]^{\mathrm{T}} \tag{9}$$

[a)] Electronic mail: mmondal@ur.rochester.edu
[b)] Electronic mail: pengfei.huo@rochester.edu

The Hamiltonian in Eq. 7 is very sparse in nature and

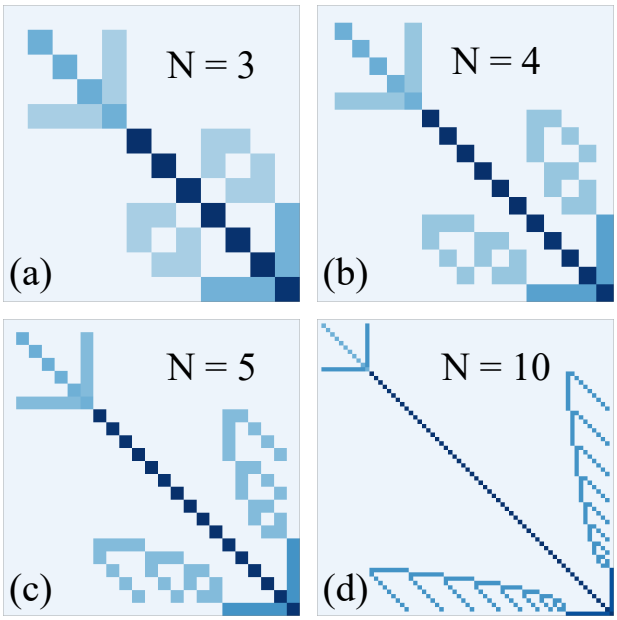

FIG. 1. HTC hamiltonian structure for N molecules. Panel (a)-(d) shows the hamiltonian for 3, 4, 5 and 10 molecules respectively under the double excitation basis

the sparsity of the Hamiltonian increases as $\mathcal{O}(N^4)$ as can be seen in Fig. 1. The action of this Hamiltonian (7), on a general wavefunction (8) can be expressed as

$$\begin{aligned}\hat{H}_{\mathrm{HTC}}\left|\Psi\right\rangle = &\sum_i (c_{\mathrm{E}_i^0}\omega_i + c_{\mathrm{G}^1}g_c)\left|\mathrm{E}_i^0\right\rangle + \\ &\left(c_{\mathrm{G}^1}\omega_c + \sum_i c_{\mathrm{E}_i^0}\omega_i\right)\left|\mathrm{G}^1\right\rangle + \\ &\sum_{i,j>i}\left\{(\omega_i+\omega_j)c_{\mathrm{E}_{ij}^0} + g_c(c_{\mathrm{E}_i^0}+c_{\mathrm{E}_j^0})\right\}\left|\mathrm{E}_{ij}^0\right\rangle + \\ &\sum_i\left\{g_c\sum_{j>i}c_{\mathrm{E}_{ij}^0} + (\omega_i+\omega_c)c_{\mathrm{E}_i^1} + \sqrt{2}g_c c_{\mathrm{G}^2}\right\}\left|\mathrm{E}_i^1\right\rangle + \\ &\left(2c_{\mathrm{G}^2}\omega_c + \sqrt{2}g_c\sum_i c_{\mathrm{E}_i^1}\right)\left|\mathrm{G}^2\right\rangle \end{aligned} \tag{10}$$

The above can be simply expressed as

$$\hat{H}_{\mathrm{HTC}}\left|\Psi\right\rangle = \underbrace{\left|\epsilon_\Psi\right\rangle \odot \left|\Psi\right\rangle}_{\mathrm{diagonal}} + \underbrace{g_c\left|\Phi\right\rangle}_{\mathrm{off-diagonal}} \tag{11}$$

where

$$\left|\epsilon_\Psi\right\rangle \rightarrow \begin{bmatrix} 0 \\ \epsilon_{\mathrm{E}_i^0} \\ \omega_c \\ \epsilon_{\mathrm{E}_{ij}^0} \\ \epsilon_{\mathrm{E}_i^1} \\ 2\omega_c \end{bmatrix}, \quad \left|\Phi\right\rangle \rightarrow \begin{bmatrix} 0 \\ c_{\mathrm{G}^1} \\ \sum_i c_{\mathrm{E}_i^0} \\ c_{\mathrm{E}_i^1} + c_{\mathrm{E}_j^1} \\ \sum_{j>i} c_{\mathrm{E}_{ij}^0} + \sqrt{2}c_{\mathrm{G}^2} \\ \sqrt{2}\sum_i c_{\mathrm{E}_i^1} \end{bmatrix} \tag{12}$$

The above operation is basically almost a linear scaling in the number of states, i.e., $\mathcal{O}(N^2)$ for N-molecule polaritonic systems. The final vector after the above operation is,

$$\hat{H}_{\mathrm{HTC}}\left|\Psi\right\rangle = \begin{bmatrix} 0 \\ \omega_i c_{\mathrm{E}_i^0} + g_c c_{\mathrm{G}^1} \\ \sum_i \omega_i c_{\mathrm{E}_i^0} + \omega_c c_{\mathrm{G}^1} \\ \epsilon_{\mathrm{E}_i^1} c_{\mathrm{E}_{ij}^0} + g_c(c_{\mathrm{E}_i^1} + c_{\mathrm{E}_j^1}) \\ g_c\sum_{j>i} c_{\mathrm{E}_{ij}^0} + \epsilon_{\mathrm{E}_i^1} c_{\mathrm{E}_i^1} + \sqrt{2}g_c c_{\mathrm{G}^2} \\ \sqrt{2}g_c\sum_i c_{\mathrm{E}_i^1} + 2\omega_c c_{\mathrm{G}^2} \end{bmatrix} \tag{13}$$

The simplified sparse action of $\hat{H}_{\mathrm{HTC}}$ can be used to accurately calculate electronic evolution via polynomial expansions of exponential propagators like Chebyshev series. This helps us avoid other expensive PDE methods like RK (Runge-Kutta), velocity verlet schemes which needs to broken down to a series of sub-steps leading to a large number of matrix-vector operations.

1. Chebyshev series expansion of matrix exponential

For the propagation of the electronic wavefunction with the Schrodinger equation,

$$i\hbar\frac{\partial\left|\Psi\right\rangle}{\partial x} = \hat{H}_{\mathrm{HTC}}\left|\Psi\right\rangle \tag{14}$$

the electronic propagator can be exactly written by,

$$\left|\Psi(t+\Delta)\right\rangle = e^{-i\frac{\hat{H}_{\mathrm{HTC}}\Delta}{\hbar}}\left|\Psi(t)\right\rangle \tag{15}$$

For a small nuclear time step, Δ, the above can be exactly approxiamted by Chebyshev polynomial expansion,

$$e^{-i\frac{\hat{H}_{\mathrm{HTC}}\Delta}{\hbar}}\left|\Psi\right\rangle = b_0(z)|\Psi^{(0)}\rangle + \sum_{n=1}^{\infty}\phi_n(z)b_n(z)|\Psi^{(n)}\rangle \tag{16}$$

with $|\Psi^{(0)}\rangle = |\Psi(t)\rangle$. b_n are the bessel-function coefficients of first rank and the number of coefficients required for the above expansion is dictated by

$$z = \frac{\delta_E\cdot\Delta}{2\hbar} \tag{17}$$

and for $z \leq 1$, we just need only the first few terms of the expansion. A higher time step(Δ) or a higher spectral radius(δ_E) results in a higher z value which necessisates the requirement of more number of terms in the expansion, Eq. 16. In Figure(2), we can see that with an increase in z, we need more and more terms for the expansion to converge. For, $z \ll 1$, we basically just, need just the first three terms in the expansion. In comparison to integrators like RK-4 or velocity verlet which needs nuclear time-step to be divided into atleast 10-100 grid points which can translate to roughly at least 4-8 matrix vector multiplication operations for each time grid point,

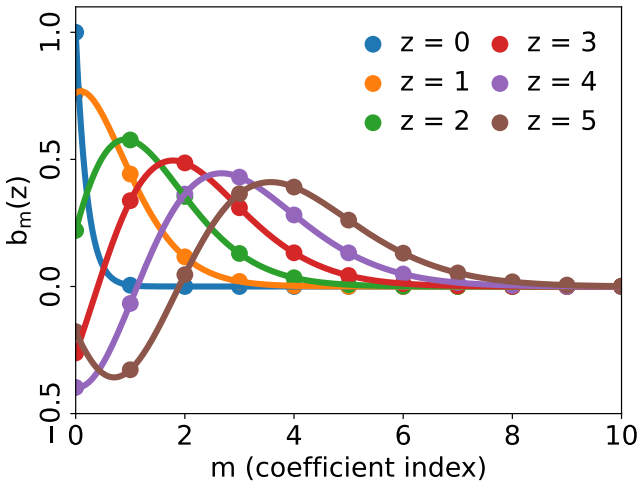

FIG. 2. The Chebyshev coefficients with varying z.

here we just need 3-4 matrix vector multiplication operation. This is a speed-up of upto 10-100 points without any loss of accuracy.

Each term in Eq. 16 is multiplied by a phase carrying information about the shift in energy axis and is given by,

$$\phi_n(z) = 2i^n e^{i\left(\frac{\delta_E}{2}+\lambda_{\min}\right)\Delta} \tag{18}$$

Here δ_E corresponds to the approximate spectral radius of $\hat{H}_{\text{HTC}}$ and $\lambda_{\min}$ is an estimate of the lowest eigenvalue of $\hat{H}_{\text{HTC}}$. The n^{th} order term in the expansion is calculated as

$$|\Psi^{(n)}\rangle = \begin{cases} \hat{O}|\Psi\rangle & n=1 \\ 2\hat{O}\left|\Psi^{(n-1)}\right\rangle - \left|\Psi^{(n-2)}\right\rangle & n \geq 2 \end{cases}$$

where $\hat{O}$ is the modified Hamiltonian,

$$\hat{O} = 2\frac{\hat{H}_{\text{HTC}} - \lambda_{\min}\hat{\mathbb{1}}}{\delta_E} - \hat{\mathbb{1}} \tag{19}$$

The action of $\hat{O}$ on $|\Psi\rangle$ is the same as in Eq. 11 with the coefficeints now scaled according to Eq. 19.

2. Seperation of excitation manifolds

The inclusion of double excitation subspace can make our δ_E to be very large which forces us to choose a very small Δ. To avoid this, we make use of the block-diagonal structure of $\hat{H}_{\text{HTC}}$. This lets us seperate the first and second exitation subspace with their individual spectral radius. The action $\hat{O}$ via Eq. 11 is thus done seperately for the different subspaces. We seperate the Hilbert space into different excitation manifolds,

$$\hat{H}_{\text{HTC}} = \hat{H}^{(0)} \oplus \hat{H}^{(1)} \oplus \hat{H}^{(2)} \tag{20}$$

$$|\Psi\rangle = |\Psi^{(0)}\rangle \oplus |\Psi^{(1)}\rangle \oplus |\Psi^{(2)}\rangle \tag{21}$$

In terms of Eq. 8,

$$|\Psi^{(0)}\rangle = c_{\text{G}^0}\left|\text{G}^0\right\rangle \tag{22}$$

$$|\Psi^{(1)}\rangle = \sum_i c_{\text{E}_i^0}\left|\text{E}_i^0\right\rangle + c_{\text{G}^1}\left|\text{G}^1\right\rangle \tag{23}$$

$$|\Psi^{(2)}\rangle = c_{\text{E}_{ij}^0}\left|\text{E}_{ij}^0\right\rangle + \sum_i c_{\text{E}_i^1}\left|\text{E}_i^1\right\rangle + c_{\text{G}^2}\left|\text{G}^2\right\rangle \tag{24}$$

So we decompose the electronic propagation into manifolds as

$$\begin{aligned} e^{-i\hat{H}_{\text{HTC}}\Delta/\hbar}|\Psi\rangle =& e^{-i\hat{H}^{(0)}\Delta/\hbar}|\Psi^{(0)}\rangle \oplus e^{-i\hat{H}^{(1)}\Delta/\hbar}|\Psi^{(1)}\rangle \\ & \oplus e^{-i\hat{H}^{(2)}\Delta/\hbar}|\Psi^{(2)}\rangle \end{aligned} \tag{25}$$

The approximate spectral radius and lowest eigenvalue for the fist excitation subspace is given by,

$$\delta_E^{(1)} = 2g_c\sqrt{N} + 2\lambda_{\text{bath}} \tag{26}$$

$$\lambda_{\min}^{(1)} = \bar{\epsilon} - g_c\sqrt{N} - \lambda_{\text{bath}} \tag{27}$$

For the second excitation manifold, these get modified as [cite Joel group theory paper],

$$\delta_E^{(2)} = 2g_c\sqrt{2N-1} + 4\lambda_{\text{bath}} \tag{28}$$

$$\lambda_{\min}^{(2)} = 2\bar{\epsilon} - g_c\sqrt{2N-1} - 2\lambda_{\text{bath}} \tag{29}$$

3. Shifting of the energy axis

As we saw above, the Chebyshev expansion lets us very efficiently calculate the nuclear propagation step in our dynamics by very accurately calculating the action of the unitary propagator on an arbitrary vector. There is a small caveat here. If we look at the Eq. 18, we see the phase factor in Chebyshev expansion (Eq. 16) depends on the approximate absolute magnitude of the lower eigenvalue. Thus, if the eigenvalue itself is very high in absolute magnitude, the accuracy of this method goes down due to noise building up from high oscillatory term coming from the high absolute magnitude of $\lambda_{\min}$, especially if we are looking at electronic excitations where these values are in orders of eV. To resolve this issue, we rewrite the Hamiltonian structure in Eq. 20 as

$$\begin{aligned} \hat{H}_{\text{HTC}} &= \hat{H}^{(0)} \oplus \hat{H}^{(1)} \oplus \hat{H}^{(2)} \\ &= \hat{H}^{(0)} \oplus (\bar{\epsilon}\hat{\mathbb{1}} + \hat{\delta}_H^{(1)}) \oplus (2\bar{\epsilon}\hat{\mathbb{1}} + \hat{\delta}_H^{(2)}) \end{aligned} \tag{30}$$

Using this, the propagator now becomes,

$$\begin{aligned} e^{-i\hat{H}_{\text{HTC}}\Delta/\hbar}|\Psi\rangle =& e^{-i\hat{H}^{(0)}\Delta/\hbar}|\Psi^{(0)}\rangle \\ & \oplus e^{-i\bar{\epsilon}\Delta/\hbar}\left\{e^{-i\hat{\delta}_H^{(1)}\Delta/\hbar}|\Psi^{(1)}\rangle\right\} \\ & \oplus e^{-2i\bar{\epsilon}\Delta/\hbar}\left\{e^{-i\hat{\delta}_H^{(2)}\Delta/\hbar}|\Psi^{(2)}\rangle\right\} \end{aligned} \tag{31}$$

This simple rearrangement, shifts the lower eigenvalues of the different manifolds from an absolute scale of $\bar{\epsilon}$, electronic excitation energies, to a relative scale of Ω_c, the

Rabi splitting of upper and lower polaritons. Thus, the accuracy of the Chebyshev propagator is now independent of the electronic excitation energies. The approximate lower eigenvalues of the two manifolds to be used in Chebyshev expansion become

$$\lambda_{\min}^{(1)} = -g_c\sqrt{N} - \lambda_{\text{bath}} \tag{32}$$

$$\lambda_{\min}^{(2)} = -g_c\sqrt{2N-1} - 2\lambda_{\text{bath}} \tag{33}$$

This significantly reduces noise and thus increasing the accuracy of the Chebyshev expansion method.

B. $\mu\Psi$

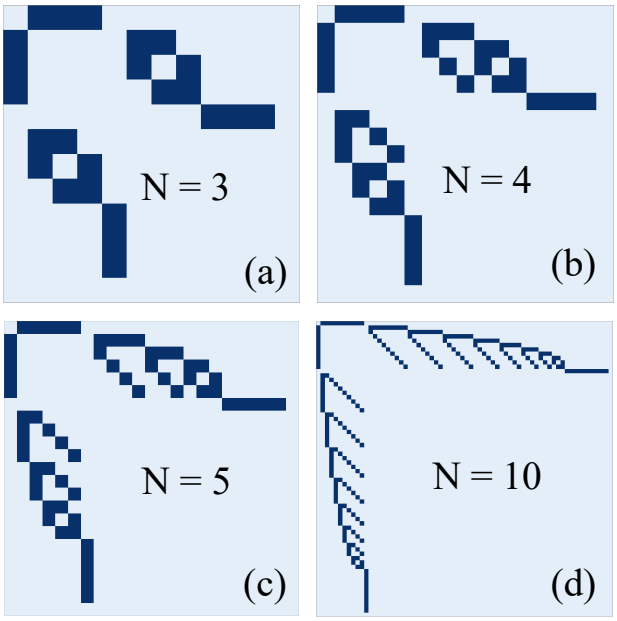

FIG. 3. HTC hamiltonian structure for N molecules. Panel (a)-(d) shows the Hamiltonian for 3, 4, 5 and 10 molecules respectively under the double excitation basis

We can write the matter dipole operator in the double-excitation subspace as,

$$\begin{aligned}\hat{\mu} = \sum_i \mu_i \left(|\mathrm{G}^0\rangle\langle \mathrm{E}_i^0| + |\mathrm{G}^1\rangle\langle \mathrm{E}_i^1| + h.c.\right) \\ + \sum_{i,j>i} \mu_j \left(|\mathrm{E}_i^0\rangle\langle \mathrm{E}_{ij}^0| + h.c\right)\end{aligned} \tag{34}$$

The action of μ on the wavevector Eq. 8 can be written as,

$$\begin{aligned}\hat{\mu}\Psi = \sum_i \mu_i c_{\mathrm{E}_i^0} |\mathrm{G}^0\rangle + \sum_i \left(\mu_i c_{\mathrm{G}^0} + \sum_{j>i} \mu_j c_{\mathrm{E}_{ij}^0}\right) |\mathrm{E}_i^0\rangle \\ + \sum_i \mu_i c_{\mathrm{E}_i^1} |\mathrm{G}^1\rangle + c_{\mathrm{G}^1} \sum_i \mu_i |\mathrm{E}_i^1\rangle\end{aligned} \tag{35}$$

The above becomes a very simplified modification of Ψ,

$$\hat{\mu}\Psi = \begin{bmatrix} \sum_i \mu_i c_{\mathrm{E}_i^0} \\ \mu_i c_{\mathrm{G}^0} + \sum_{j>i} \mu_j c_{\mathrm{E}_{ij}^0} \\ \sum_i \mu_i c_{\mathrm{E}_i^1} \\ \sum_{i<j} \mu_i c_{\mathrm{E}_{ij}^0} \\ \mu_i c_{\mathrm{G}^1} \\ 0 \end{bmatrix} \tag{36}$$

We can see that the above is just a simple rearrangement of $\hat{\mu} \odot \Psi$. This helps simplify a lot of dipole operations.

1. Focusing $\mu\Psi$

The PLDM algorithm for 2DES requires us to focus on the most important element after the action of each laser pulse. This is done by the importance sampling procedure. The application of a laser at a given time on the system can be represented by the dipole operator acting on the system density matrix for a trajectory. We can expand this as,

$$\hat{\mu}\hat{\rho} = \tilde{\rho} = \sum_{ab} \rho_{ab} |a\rangle\langle b| = \sum_{ab} r_{ab} e^{i\theta_{ab}} |a\rangle\langle b| \,. \tag{37}$$

This can be thought of as elementwise multiplication of two matrices R and P containing the magnitudes and phases of $\tilde{\rho}$.

$$\hat{r} = \sum_{ab} r_{ab} |a\rangle\langle b| \quad , \quad \hat{\theta} = \sum_{ab} e^{i\theta_{ab}} |a\rangle\langle b| \tag{38}$$

The Cumulative Distribution Function (CDF) is generated from the absolute value of this density matrix,

$$\hat{D} = \sum_{ab} d_{ab} |a\rangle\langle b| \tag{39}$$

where,

$$d_{ab} = \sum_{\substack{m\le a \\ n\le b}} r_{mn}. \tag{40}$$

Defining,

$$R = \sum_{ab} r_{ab} \tag{41}$$

we use the normalised CDF for the focusing step[?] . We sample a uniform random number, ζ, and select the collective index $K \equiv ab$, where

$$\frac{d_{K-1}}{R} < \zeta \le \frac{d_K}{R} \tag{42}$$

To get $\tilde{\rho}$, we must multiply two $\mathcal{O}(N^4)$ size matrices and further, from Eq.40, to calculate the CDF of this large matrix we need to perform another $\mathcal{O}(N^4)$ operation on $\tilde{\rho}$. This makes our computation both time and memory

requirements exponentially blow up with increase in the number of molecules in the HTC Hamiltonian.

The forward-backward nature of PLDM can be used at this stage to simplify this issue. Within the PLDM framework, for a single trajectory, the system density matrix can be represented as the outer product of a "forward" and a "backward" wavefunction.

$$\hat{\rho} = |\Psi_F\rangle\langle\Psi_B| \tag{43}$$

The operation of the dipole operator can thus be rewritten as

$$\hat{\mu}\hat{\rho} = \hat{\mu}\,|\Psi_F\rangle\langle\Psi_B| = (\hat{\mu}\,|\Psi_F\rangle)\,\langle\Psi_B| = |\Phi_F\rangle\langle\Psi_B| \tag{44}$$

where $|\Phi_F\rangle = \hat{\mu}\,|\Psi_F\rangle$, can be obtained from Eq. 36. If we consider,

$$|\Phi_F\rangle = \sum_a c_a\,|a\rangle = \sum_a r_a e^{i\theta_a}\,|a\rangle \tag{45}$$

we can construct a vector of magnitudes for $|\Phi_F\rangle$ as,

$$|r_F\rangle = \sum_a r_a\,|a\rangle \tag{46}$$

Similarly, we define $\langle R_B|$ as the vector of magnitudes of $\langle\Psi_B|$. Since the calculation of CDF only involves the absolute magnitudes density matrix elements, we can show that the matrix $\hat{R}$ in Eq. 38 can be rewritten as

$$\hat{r} = |r_F\rangle\langle r_B| = \sum_{ab} r_a r_b\,|a\rangle\langle b| = \sum_{ab} r_{ab}\,|a\rangle\langle b| \tag{47}$$

Beacuse of the outer product of magnitudes, the sum over all elements can now be simplified as,

$$R = \sum_{ab} r_{ab} = \left(\sum_a r_a\right)\left(\sum_b r_b\right) = R_F R_B \tag{48}$$

where $R_F = \sum_a r_a$ and similar for R_B. We also define the cumulative sum along $|r_F\rangle$ as

$$|D_F\rangle = \sum_a d_a\,|a\rangle \tag{49}$$

where

$$d_a = \sum_{m\le a} r_m \tag{50}$$

Similarly we also define a CDF along $\langle r_b|$ as $\langle D_B|$. Searching for the forward index is equivalent to the search of the row of the focused element. We try to search for row p, for which Eq. 42 is satisfied. So we search for the index with

$$\frac{d_{ab}}{R} \ge \zeta \tag{51}$$

Now $d_{ab} \le d_a R_b$. Thus, we search for,

$$\frac{d_a R_b}{R} \ge \zeta \tag{52a}$$

$$\frac{d_a R_b}{R_a R_b} \ge \zeta \tag{52b}$$

$$\frac{d_a}{R_a} \ge \zeta \tag{52c}$$

So just comparing ζ with the normalised $\langle D_B|$ will give us the backward index. Suppose we got the forward index as p, we search for the backward index by expanding Eq. 51 in terms of the individual components defined in Eq. 50,

$$\frac{1}{R}\left(d_b r_p + \langle D_B|p-1\rangle\, R_b\right) \ge \zeta \tag{53}$$

2. Final response function

If we want to calculate the n^{th} order response, it will of the form

$$R^{(n)} = \mathrm{Tr}[\hat{\mu}\hat{\rho}^{(n)}] \tag{54}$$

For, forward-backward trajectory methods, we can directly use Eq. 44 to get the form,

$$R^{(n)} = \mathrm{Tr}[|\Phi_F\rangle\langle\Psi_B|] = \langle\Psi_B|\Phi_F\rangle \tag{55}$$

This is basically the scalar product between the two wavefunctions. Thus, we end up with not generating the full density matrix of $\mathcal{O}(N^4)$ for computing the response for forward-backward methods.

C. Vectorising over t_3 and trajectories

Simulating 2DES itself can be really expensive as it scales as $\mathcal{O}(T^3)$ with T being the number of propagation steps after a single laser. Along with this, for a N-molecule polaritonic system, the inclusion of 2^{nd} excitation manifold leads to a $\mathcal{O}(N^2)$ number of states and the density matrix becomes $\mathcal{O}(N^4)$. The full-density matrix dynamics will invlove compuatation with $\mathcal{O}(N^5)$ operations. The total cost of 2DES simulation for N-molecule polaritonic system, for M trajectories, thus becomes $\mathcal{O}(N^5T^3M)$. This scaling is both memory and time intensive and so the simulation of a large N systems seems unrealistic. But, using the strategies developed in the previous sections, we saw that we actually never need to generate any $\mathcal{O}(N^4)$ density matrix and all of our calculations can be done with vectors of $\mathcal{O}(N^2)$. The matrix-vector and matrix-matrix multiplications reduced to simple Hadamard products, reduces the density matrix dynamics from $\mathcal{O}(N^5)$ to just $\mathcal{O}(N^2)$.

Since each of the trajectory is independent, the simulation can be parallelised over the M trajectories. This drastically already reduces our computation to $\mathcal{O}(N^2T^3)$.

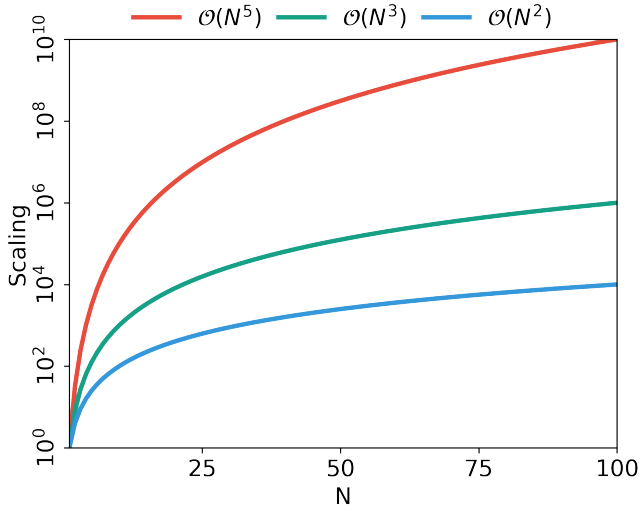

FIG. 4. 2DES computational cost scaling with increasing number of molecules.

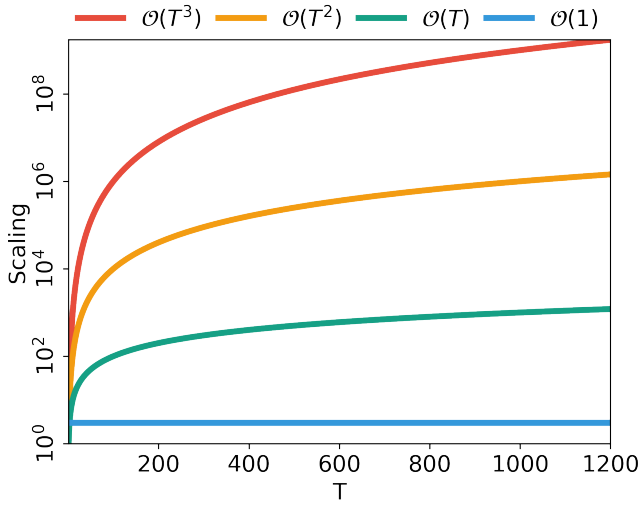

FIG. 5. 2DES computational cost scaling with increasing number of time steps for each laser pulse waiting time.

Now, we can further make use of the simplified Hadamard products to vectorise our code over each of the laser runs which can in-principle remove the scaling over T and our computation can thus be reduced to the cost of $\mathcal{O}(N^2)$.

The vectorisation can be carried out for each laser step seperately by the simple procedure below,

$$\Psi = \begin{bmatrix} \vdots & & \vdots \\ \psi_1 & \cdots & \psi_T \\ \vdots & & \vdots \end{bmatrix} \xrightarrow{e^{-i\hat{H}\Delta/\hbar}} \begin{bmatrix} \vdots & & \vdots \\ \psi_1^{\Delta} & \cdots & \psi_T^{\Delta} \\ \vdots & & \vdots \end{bmatrix} = \Psi(\Delta) \tag{56}$$

where ψ_i is basically the modified wavefunction after the application of laser at time step t_i and ψ_i^{Δ} is the propagation of ψ_i for time step Δ. During the dynamics, all the matrix vector operations can be very simply vectorised. For example, the diagonal part in Eq. 11 can now be very simply evaluated as the following Hadamard product

$$\begin{aligned} |\epsilon\rangle \odot |\Psi\rangle \rightarrow \begin{bmatrix} \vdots & & \vdots \\ \epsilon_1 & \cdots & \epsilon_T \\ \vdots & & \vdots \end{bmatrix} \odot \begin{bmatrix} \vdots & & \vdots \\ \Psi_1 & \cdots & \Psi_T \\ \vdots & & \vdots \end{bmatrix} \\ = \begin{bmatrix} \vdots & & \vdots \\ \epsilon_1\Psi_1 & \cdots & \epsilon_T\Psi_T \\ \vdots & & \vdots \end{bmatrix} \end{aligned} \tag{57}$$

The psoition(R) and momenta(P) of the bath degrees of freedom can be similary vectorised as

$$\mathbf{R} = \begin{bmatrix} \vdots & & \vdots \\ R_1 & \cdots & R_T \\ \vdots & & \vdots \end{bmatrix} \xrightarrow{\partial_R = \nabla_R \hat{H}\Psi} \begin{bmatrix} \vdots & & \vdots \\ R_1^{\Delta} & \cdots & R_T^{\Delta} \\ \vdots & & \vdots \end{bmatrix} = \mathbf{R}(\Delta) \tag{58}$$

The above vectorization is very general and in principle, can be applied to wavefunctions propagating independently. So the wavefunctions from different trajectories can also be combined to further reduce the cost. As a reverse strategy, different wavefunction propagation (after the application of a laser) within a trajectory can be treated as different trajectories and the dynamics can then be parallelized over these wavefunctions. So, the above represents a combined strategy to speed up non-linear spectroscopy calculations for N-molecule polaritonic systems described by the HTC Hamiltonian using both vectorization and parallelization over wavefunctions.

D. Results

1. Linear Spectra

We simulate the linear absorption spectra for 500 molecules for various energetic and orientational disorders. We chose a homogenous energy disorder where the static inhomogeneous distribution of site energies has been sampled from a gaussian distribution given by,

$$P(\epsilon_n) = \frac{1}{\sqrt{2\pi\sigma_\epsilon^2}} e^{-(\epsilon_n - \bar{\epsilon})/2\sigma_\epsilon^2} \tag{59}$$

In Fig. 6, we show the Linear absorption of 500 molecules under various energy disorder. Fig. 6(a) is the absorption normalized with area and Fig. 6(b) is the absorption normalized with the absorption peak intensity for each disorder. We can see that as the disorder in energy (σ_ϵ) approaches the order of Rabi-splitting(Ω),

1. Peak intensity decreases. This is beacuse the effective number of molecules with zero detuning decreases

2. Effective Rabi-splitting slightly increases. This is beacuse is because of the increased inhomogenity in the sample.

3. The linewidth of upper and lower polaritons widens and with increased disorder, the Rabi-splitting fades away. This pattern is clearer when we normalise the curves with the maximum peak intensity in Fig. 6(b).

A dipole disorder has been introduced by sampling the molecule orientation with respect to the cavity mode by sampling angles from a gaussian distribution

$$P(\theta_n) = \frac{1}{\sqrt{2\pi\sigma_\theta^2}} e^{-(\theta_n - \bar{\theta})/2\sigma_\theta^2} \tag{60}$$

The orientational disorder effects in the light matter coupling by introducing

$$g_{\rm c} \rightarrow g_{\rm c}\cos(\theta_n) \tag{61}$$

in the Eqn. 62 such that,

$$\hat{H}_{\rm HTC} = \sum_i \hbar\omega_i \hat{\sigma}_i^\dagger \hat{\sigma}_i + \hbar\omega_{\rm c}\hat{a}^\dagger\hat{a} + \hbar g_{\rm c}\sum_i \cos(\theta_i)(\hat{\sigma}_i^\dagger\hat{a} + \hat{\sigma}_i\hat{a}^\dagger) \tag{62}$$

The orientation disorder can correspond to certain phases in different materials and in the limit of infinite disorder we have a random orientation of molecules in a solution.

In Fig. 7, we present the linear spectra of 500 molecules coupled to a single cavity mode under various dipole disorders. With an increased disorder,

1. The effective Rabi-splitting decreases until it converses to a specific Ω irrespective of the amount of disorder. Fig. 7 shows that the convergence is reached around a disorder of with 90^0. In Fig. 7(b), we see that the uniform convergence corresponds to the Rabi-splitting of

$$\Omega_{\rm eff} = \left\{ \left(\frac{\Omega}{\sqrt{2}}\right)^2 + \left(\lambda - i\left[\sqrt{(\ln 2)\mathrm{k_B T}} - \frac{\Gamma}{2}\right]\right)^2 \right\}^{\frac{1}{2}} \tag{63}$$

where a $\sqrt{2}$ factor in the first term accounts for the average of $\cos^2(\theta)$ in a 2-dimensional system.

2. The linewidth of the polariton peaks remain unchanged as we are not adding any additional broadening mechanisms (like inhomogenous energetic disorder or additional loss channels) in the system.

2. 2DES

To demonstrate the feasibility of 2DES simulations with large N, we simulate the 2DES of N-molecule HTC-system for various N at a fixed cavity loss rate. The molecular parameters are kept same as in the linear spectra simulations. Due to the inclusion of doubly excited subspace, the total number of electronic states now scale as $\approx \mathcal{O}(N^2)$. Fig. 8 shows the pure-absorptive 2DES for various N at $t_2 = 0$fs for a fixed Rabi-splitting, $\Omega_{\rm R}$.

Fig. 8(a)-(d) shows the rephasing signal for different values of N. The diagonal peaks correspond to the upper and lower polariton states and the cross-peaks correspond to the coherence between these polaritonic states. With increasing N, we can observe a significant reduction in the linewidth of various peaks as was visible from the linear spectra also.

In Fig. 8(e)-(h), we present the non-rephasing response signal intensity for different N. We can distinctly observe the appearance of cross-peak with $N = 2$ and this signal intensifies relative to cross-peaks with larger N. With increasing N, we thus have more pathways tranfering coherences through the non-rephasing pathways as well.

In Fig. 8(i)-(l), we present the total pure-absorptive spectra for different N. As we compare the lineshapes, we see that, as the N gets larger, the signal becomes more homogenous and so the total signal is mostly dominated by non-rephasing pathways.

III. CONCLUSION

ACKNOWLEDGMENTS

This work was supported by the Department of Energy under Grant No. DE-SC0022171. P.H. appreciates the support from his Cottrell Scholar Award (a program by the Research Corporation for Science Advancement). Computing resources were provided by the Center for Integrated Research Computing (CIRC) at the University of Rochester. The authors appreciate valuable discussions and comments from Benjamin Chng.

SUPPLEMENTARY MATERIAL

CONFLICT OF INTEREST

The authors have no conflicts to disclose.

AVAILABILITY OF DATA

The data that support the findings of this work are available from the corresponding author under reasonable request.

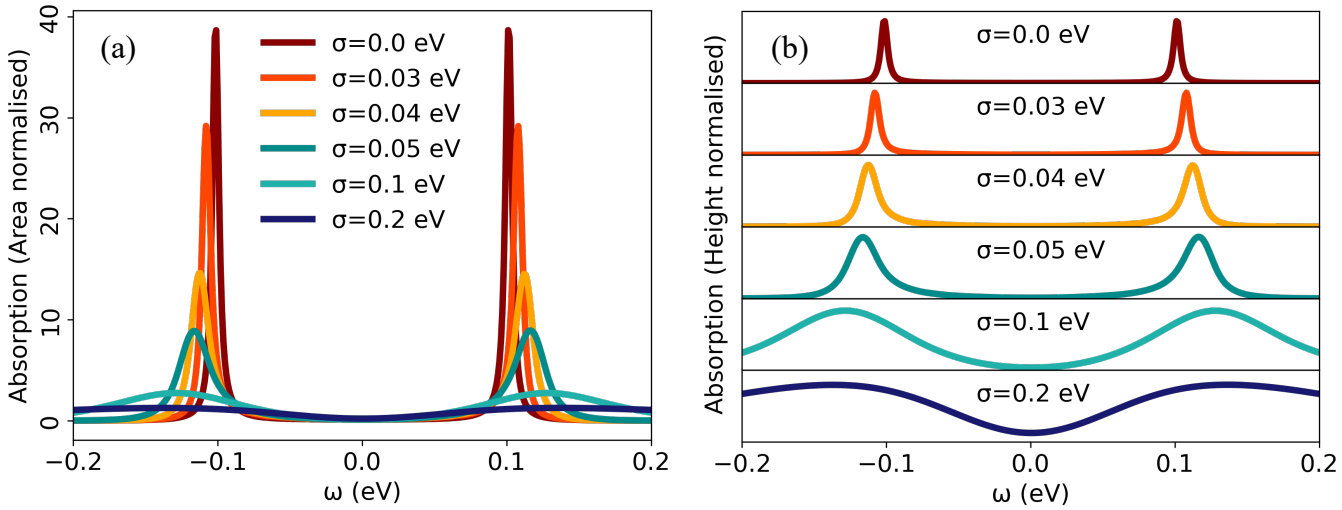

FIG. 6. Linear spectra of 500 molecules in presence of various energy disorders. (a) Polariton absorption spectra with each curve being normalised with the corresponding area and (b) represents the absorption curves with the height being normalised.

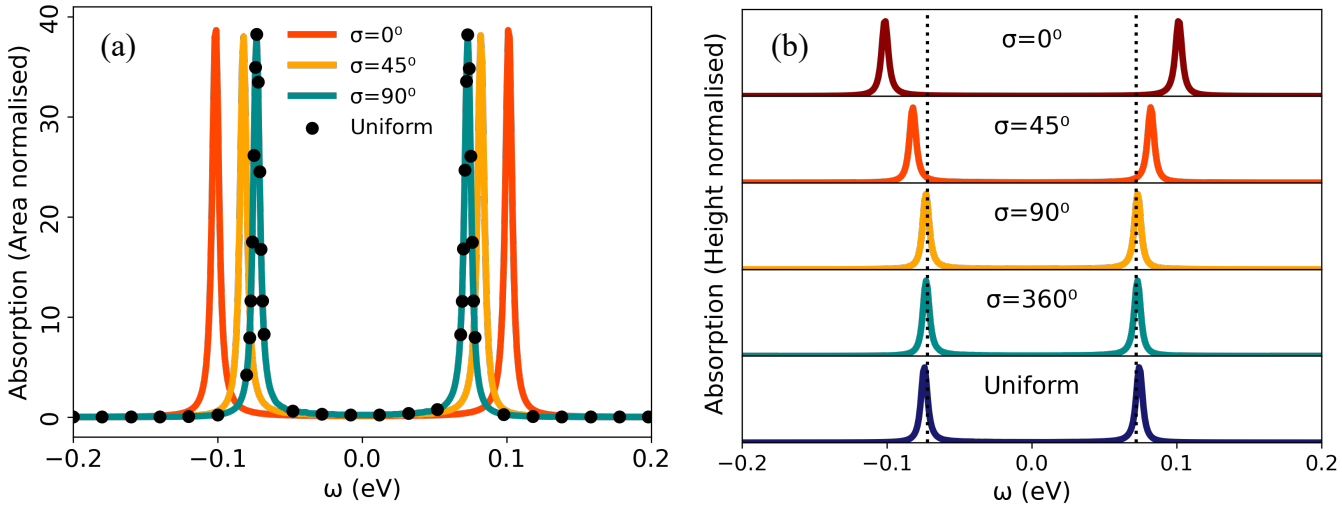

FIG. 7. Linear spectra of 500 molecules in presence of various dipole disorders. (a) Polariton absorption spectra with each curve being normalised with the corresponding area and (b) represents the absorption curves with the height being normalised.

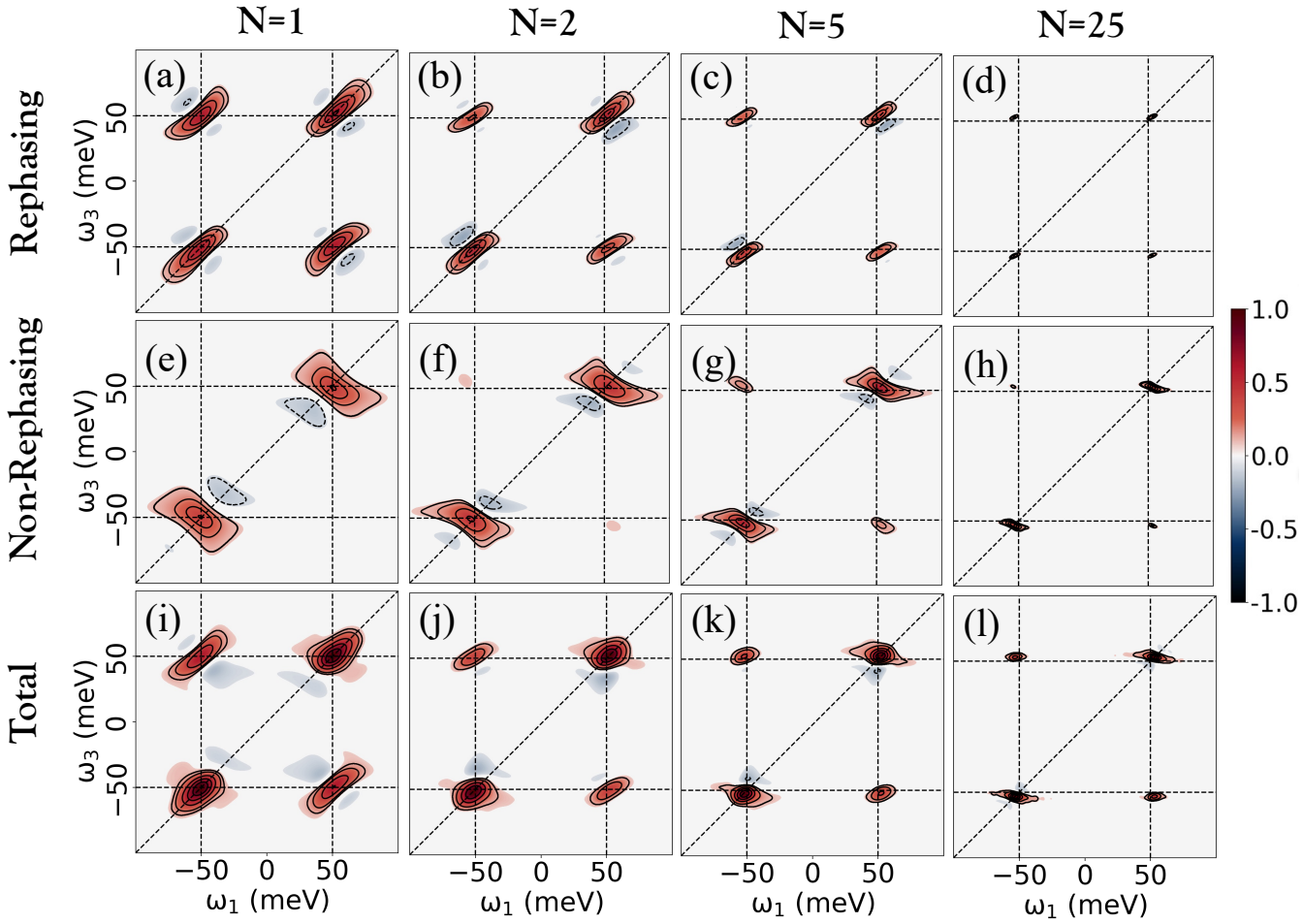

FIG. 8. Pure absorptive spectra breakdown for polaritonic systems containing various number of molecules. Panels (a)-(d) represents the rephasing spectra. Panels (e)-(f) show non-rephasing spectra and panels (i)-(l) show the total pure-absorptive spectra for different N.